This is an open access article published under an ACS AuthorChoice License, which permits copying and redistribution of the article or any adaptations for non-commercial purposes.

Downloaded via UNIV OF MILAN on February 9, 2022 at 11:54:25 (UTC).
See https://pubs.acs.org/sharingguidelines for options on how to legitimately share published articles.

ARTICLE

Charge Transport in Nanoscale "All-Inorganic" Networks of Semiconductor Nanorods Linked by Metal Domains

Romain Lavieville,[†,§] Yang Zhang,[†,§] Alberto Casu,[†] Alessandro Genovese,[†] Liberato Manna,[†] Enzo Di Fabrizio,[†,‡] and Roman Krahne[†,*]

[†]Istituto Italiano di Tecnologia (IIT), Via Morego 30, 16163 Genova, Italy and [‡]BIONEM Lab, University of Magna Graecia Campus S. Venuta, viale Europa, 88100 Catanzaro, Italy. [§]These authors contributed equally to this work.

ABSTRACT Charge transport across metal-semiconductor interfaces at the nanoscale is a crucial issue in nanoelectronics. Chains of semiconductor nanorods linked by Au particles represent an ideal model system in this respect, because the metal–semiconductor interface is an intrinsic feature of the nanosystem and does not manifest solely as the contact to the macroscopic external electrodes. Here we investigate charge transport mechanisms in all-inorganic hybrid metal–semiconductor networks fabricated *via* self-assembly in solution, in which CdSe nanorods were linked to each other by Au nanoparticles. Thermal annealing of our devices changed the morphology of the networks and resulted in the removal of small Au domains that were present on the lateral nanorod facets, and in ripening of the Au nanoparticles in the nanorod junctions with more homogeneous metal-semiconductor interfaces. In such thermally annealed devices the voltage dependence of the current at room temperature can be well described by a Schottky barrier lowering at a metal semiconductor contact under reverse bias, if the spherical shape of the gold nanoparticles is considered. In this case the natural logarithm of the current does not follow the square-root dependence of the voltage as in the bulk, but that of $V^{2/3}$. From our fitting with this model we extract the effective permittivity that agrees well with theoretical predictions for the permittivity near the surface of CdSe nanorods. Furthermore, the annealing improved the network conductance at cryogenic temperatures, which could be related to the reduction of the number of trap states.

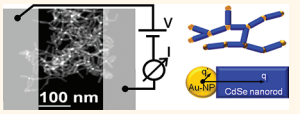

KEYWORDS: metal–semiconductor nanojunction · self-assembly · networks · charge transport · Schottky–Richardson model · thermionic emission

Colloidal semiconductor nanorods provide an innovative approach to nanoscale electronic devices with size-dimensions that are difficult to achieve *via* conventional top-down fabrication methods.[1−3] Nanorods[4] have the advantage over spherical nanoparticles in the sense that their elongated shape extends the possibilities to tune their physical properties and facilitates contact fabrication. Nowadays, nanorods with controlled shape and composition can be reproducibly fabricated *via* wet-chemical synthesis.[5,6] Toward electrical devices the properties of the electrical contacts to the nanorods play a crucial role, and the control over the latter remains a challenge. One method consists in top-down fabrication of the electrical leads *via* electron-beam lithography (EBL), which led to tunneling contacts to the nanorods and single electron transistor behavior.[7−9] However, this approach is not suitable for large scale fabrication and puts extremely high demands on the precision of the lithography process. Another possibility is the fabrication of the electrical contacts by electron- or ion-beam induced deposition, which results in strong coupling between the electrodes and the nanorod that could be modeled by Fowler–Nordheim tunneling.[10,11] Also this method is based on slow and costly lithography processes and therefore is not suitable for large-scale device fabrication.

Recently, hybrid metal–semiconductor nanocrystal structures were fabricated by wet chemistry that provided a completely different alternative to realize the electrical contacts to the semiconductor nanorods. In particular, hybrid gold–semiconductor nanodumbbells, that is, CdSe nanorods with Au domains at their tips that constitute an all-inorganic metal–semiconductor interface were synthesized.[12,13] Scanning tunneling spectroscopy on a single nanodumbbell revealed that the nanorods maintained their bandgap at the rod center, while the Au domains at their tips showed Coulomb blockade effects corresponding to their size, and found evidence of midgap states near the metal-semiconductor interface.[14] The electrical properties of such nanodumbbells were also investigated using EBL-defined electrodes as contacts and showed an increased conductivity and an electrical behavior that could be interpreted in terms of Schottky contacts.[15] The nature of the metal-semiconductor contact at the nanoscale is still under debate, since Schottky barriers in bulk systems typically

* Address correspondence to Roman.krahne@iit.it.

Received for review October 19, 2011 and accepted March 9, 2012.

Published online March 09, 2012
10.1021/nn3006625

© 2012 American Chemical Society

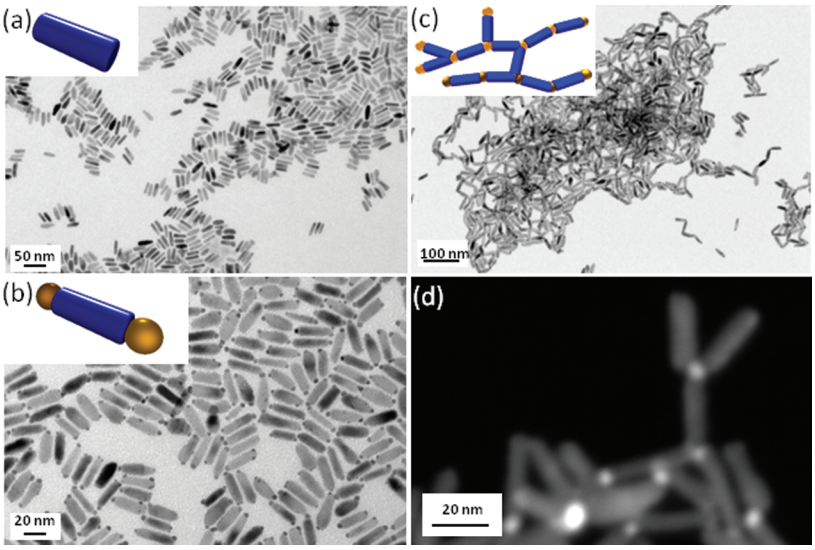

Figure 1. Transmission electron microscopy (TEM) images showing the different stages of a typical synthesis of (a) CdSe nanorods, (b) nanorods with gold domains at their tips, and (c) nanorod networks linked by gold domains. (d) High-angle annular dark field (HAADF) scanning transmission electron microscopy image displaying the nanorods and the higher contrast Au domains acting as junctions. The nanorods were ~30 nm in length and the gold spheres had an average diameter of 3 nm before annealing. The size of individual networks typically varied from hundreds of nanometers to a few micrometers in diameter.

extend over hundred nanometers or more. Theoretical modeling of lateral metal contacts to semiconductor nanorods or nanowires resulted in modifications of the electronic level structure of the nanorods in the vicinity of the metal.[16−18] One possible approach toward nanorod-based macroscale electrical devices is based on the self-assembly of nanorods on planar substrates, and various studies have investigated the electrical properties of such films of self-assembled nanorods.[19−21] However, by using planar electrode geometries on such films so far no charge injection from the electrodes was observed and only photocurrent signals were measured.[22−24] Recently, layers of vertically oriented nanorods based on cadmium chalcogenides materials have been electrically contacted in a sandwich geometry, where the conductivity could be modified by cation exchange, for example from Cd to Cu.[25,26]

A significant step toward nanoscale devices *via* self-assembly methods was the fabrication of all-inorganic nanorod networks in solution linked *via* gold domains as demonstrated by Figuerola *et al*.[27,28] Such networks promise enhanced charge injection due to the Au domains enabling conduction in the dark, and can span sizes from several hundred nanometers up to some micrometers, which significantly reduces the challenges related to the electrode fabrication and also facilitates the scale-up of the devices. Another advantage is the "all-inorganic" architecture of networks, which avoids the instability in electrical properties that is usually induced by the organic ligands linking the nanocrystals. Furthermore, nanorod networks could be exploited in more complex electrical configurations, for example, by using them as random resistor networks with multiple external contacts. In this work we investigate the electrical properties (both at room and at cryogenic temperatures) of all-inorganic networks consisting of CdSe nanorods that were linked *via* Au nanoparticles at their tips. The networks were selectively positioned onto specific interdigitated electrodes by drop deposition from solution followed by dielectrophoresis. Before thermal annealing treatment also the lateral facets of the nanorods were decorated by small Au domains, and localized trap states contributed to the conduction in the rods. Thermal annealing resulted in ripening of the Au nanoparticles in the junctions at the expense of the ones on the lateral facets. After annealing, the current−voltage ($I-V$) curves at room temperature could be well fitted with the Schottky-Richardson model that considers the spherical form of the Au nanoparticles for the barrier lowering due to the image charges. At cryogenic temperatures the current of the network devices was dominated by charge tunneling, which was actually suppressed at low bias voltage, possibly due to Coulomb charging of the Au domains at the nanorod tips.[14] Annealed networks showed an improved conductivity at low temperatures, and the current depended on voltage exponentially for external electric fields larger than 2×10^5 V/cm.

RESULTS AND DISCUSSION

We synthesized CdSe nanorods (see Figure 1a) following the seeded growth approach according to a previously published protocol.[6] Then we grew Au domains on the nanorod tips and obtained nano dumbells as displayed in Figure 1b, in which the metal and semiconductor materials formed a direct inorganic

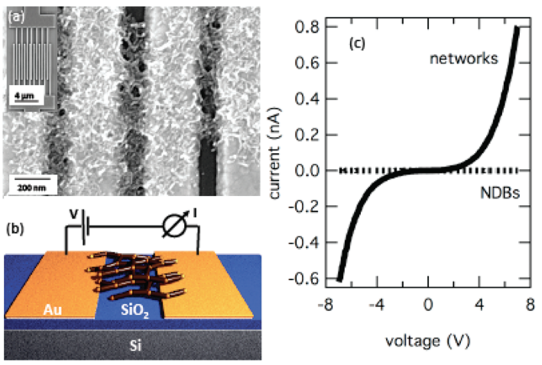

Figure 2. (a) SEM image of networks trapped by dielectrophoresis on interdigitated electrodes. The inset shows the full area of the interdigitated electrodes (with 180 nm electrode separation) before trapping. (b) Scheme of the electrical setup used in the experiments. Some networks bridge the electrode gap and provide conductive paths. (c) Typical dark *I*−*V* characteristics recorded before annealing of nanowelded CdSe nanorod networks, and of nanodumbbells at comparable nanoparticle concentration at room temperature.

interface.[12,13] Due to the high reactivity of the polar facets located at the tips of the semiconductor nanorods, the metal domains formed primarily at the nanorod tips. However, at elevated concentrations of the gold precursor used for growing the Au tips we also observed the formation of small Au domains at the lateral facets of the nanorods, as shown in Figure 3a. The networks were fabricated by destabilizing the Au domains at the nanorod tips upon addition of molecular iodine (I_2), which induced the coalescence of Au domains belonging to different nanorods and led to the formation of larger Au particles. In this way two or more nanorods[27] could be joined at their tips by a single Au domain, and micrometer size nanorod networks linked by robust and all-inorganic junctions were thus obtained (see Figure1c,d).

The nanorod networks were deposited from solution onto interdigitated electrode structures by dielectrophoresis (see Methods section). Figure 2 shows a scanning electron microscopy (SEM) image of four interdigitated electrodes covered with the networks at a typical density. The inset displays the entire interdigitated electrode region without nanocrystal coverage. We note that the nanocrystals were solely deposited onto the electrode structures to which a voltage bias was applied, thus this method allowed for a selective deposition, and neighboring electrodes that were not biased remained without nanocrystals (see Supporting Information, Figure S9). Figure 2c plots the current−voltage characteristics of networks and nanodumbbells deposited under similar conditions, and with equivalent nanorod concentration in the solution, onto the interdigitated electrodes. While the networks showed appreciable conductivity with a strongly nonlinear behavior, no measurable current was detected from the nanodumbbells or the nanorods. For network devices with a rod density as in Figure 2a we can expect

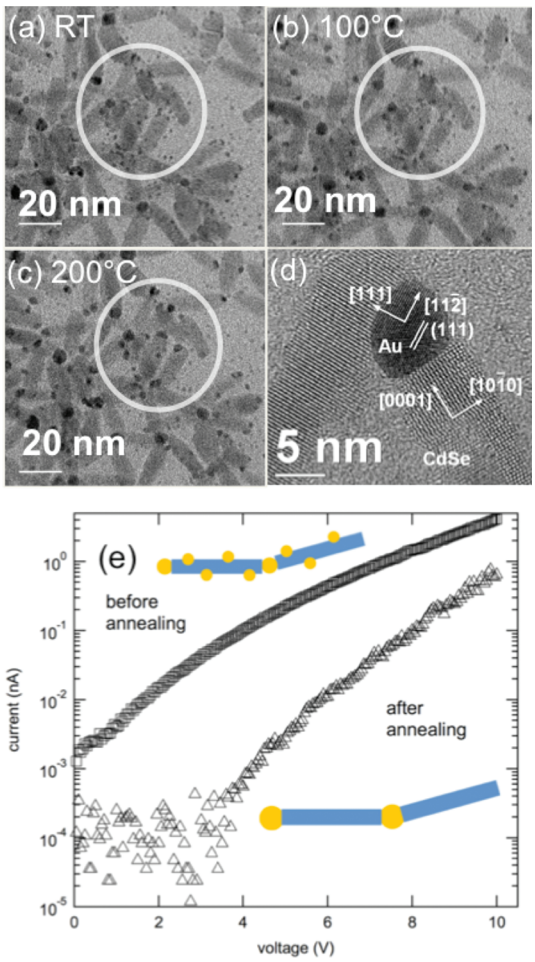

Figure 3. HRTEM images at low magnification showing the evolution of networks during the annealing experiment performed *in situ* at different temperatures: room temperature (a), 100 °C (b), and 200 °C (c). The circles highlight some regions where Au nanocrystals migrated and formed larger crystals during the annealing. (d) Typical HRTEM image displaying two CdSe nanorods linked *via* a Au nanocrystal after annealing, where the Au showed the typical (111) lattice set with periodicity of 2.35 Å. (e) Typical dark *I*−*V* characteristics of the same network devices before annealing (squares) and after annealing (triangles), both recorded at room temperature.

highly branched electrical transport pathways for the charge carriers, and that the conductance will be dominated by the nanorod chains with lowest resistance. We remark that with the interdigitated electrodes we can expect to measure several network chains in parallel.

The structure of the Au-CdSe networks could be significantly modified by thermal annealing, as already demonstrated by Figuerola *et al.* recently.[28] Figure 3(a−c) demonstrates the evolution of a network structure during thermal annealing *in situ* in a transmission electron microscope (TEM). High resolution TEM (HRTEM) investigation revealed that at room temperature the nanorods were linked at their tips by relatively small Au domains, and also a large number of even smaller Au domains at the lateral facets of the nanorods was observed. Thermal annealing in the temperature range

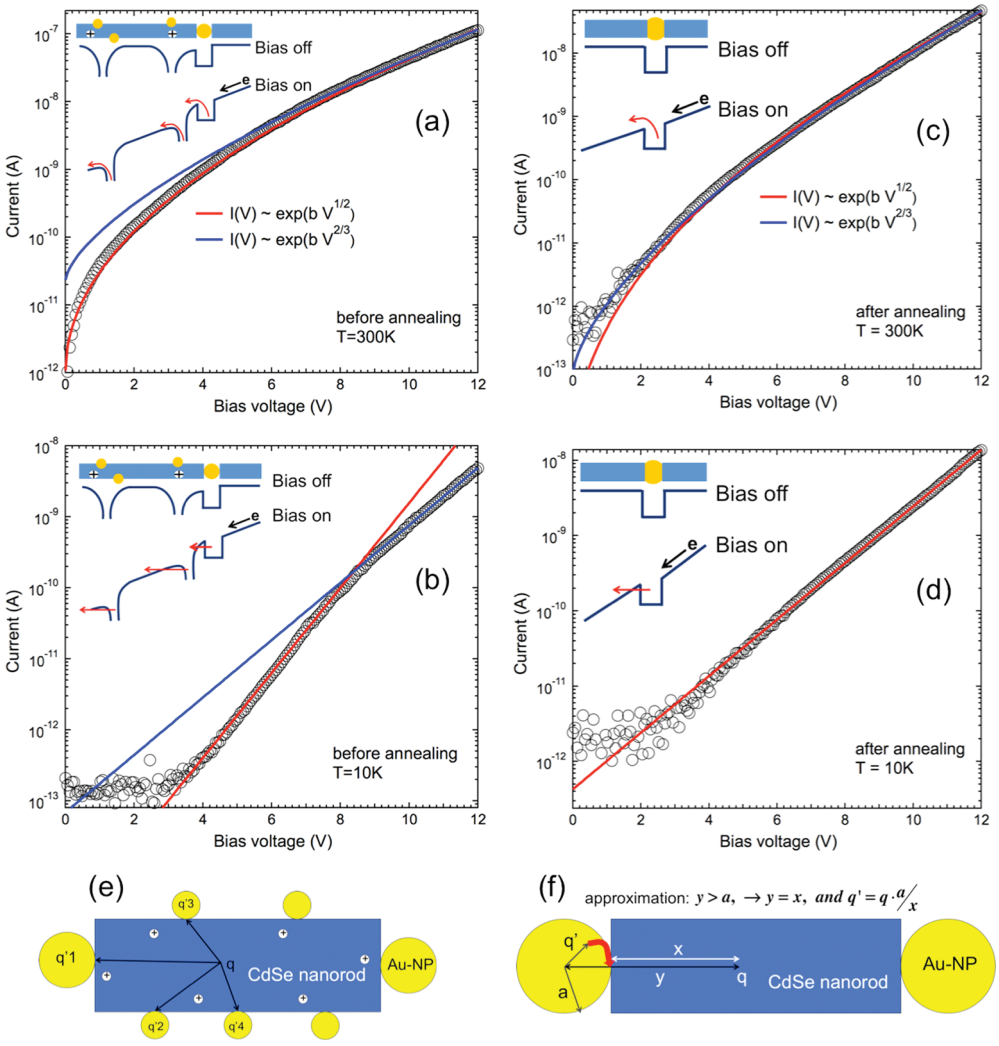

Figure 4. Current–voltage curves (open circles) recorded from a nanorod-network device before annealing (a,b) and after annealing (c,d), displayed in a semilogarithmic plot. (a,c) Room temperature behavior where the data was fitted with eqs 2 and 7, displayed by the red and blue lines, respectively. The fitting with the conducting sphere model describes the current accurately after annealing (c), and fails to describe the current voltage curve before annealing in the low bias regime (a). (b) At low temperature the *I*–*V* curve before annealing can be fitted with two different exponential functions in different voltage regimes, namely in an intermediate voltage range from 4 to 8 V (red line), and for voltage bias larger than 8 V (blue line). At low bias the current was suppressed, probably due to Coulomb blockade. (d) Current after annealing at low temperature (open circles) fitted by an exponential function (red line) that corresponds to charge tunneling (V_B = 1.16 V), as illustrated by the red arrow in the inset. Also after annealing the current was suppressed at low bias voltage due to Coulomb blockade. (e,f) Schematic illustration of the image charges before (e) and after annealing (f), the rod length is not to scale. In panel e multiple positively charged traps that might result from selenium vacancies are sketched by the plus signs. The impact of such traps might also be responsible for the $\sqrt{V}$ behavior of the current prior to annealing in addition to the contribution of the interface barriers. The red arrow in panel f illustrates the approximation for the image charge location of our model.

from 100–200 °C led to the migration of smaller Au particles toward the tips of CdSe rods, which resulted in ripening and growth of Au domains there, while the smaller Au particles at the lateral facets vanished. At the same time the Au–CdSe interfaces became more extended and in some cases a clear epitaxial relationship was found between the Au and the CdSe sections (see Supporting Information Figure S5).

The thermal annealing had also a strong effect on the electrical properties of the networks, since it resulted in a decrease of the conductivity at room temperature, as demonstrated in Figure 3e. We note that this behavior is in contrast with the results that we obtained on thin films of multibranched nanocrystals,[29,30] where annealing led to increased conductivity. The reduction in room temperature conductivity of the networks caused by annealing can be directly related to the vanishing of the small Au domains at the lateral facets of the nanorods, as we will discuss in the following in a more detailed analysis of the *I*–*V* curves obtained at room and cryogenic temperatures (see Figure 4).

For a semiconductor–metal–semiconductor structure at room temperature the current can be described by the Schottky–Richardson model of thermionic emission, and is dominated by the metal–semiconductor

junction under reverse bias, and can be expressed as[31]

$$I = A\,T^2 \exp\left(\frac{-q(\Phi_B - \Delta\Phi)}{kT}\right) \quad (1)$$

Here Φ_B is the barrier height at the metal−semiconductor interface, and $\Delta\Phi$ is the effective barrier lowering in an external electric field due to the image force, T is the temperature, k is the Boltzmann constant, and A is the effective Richardson constant. For a bulk junction, and by assuming a constant electric field $E = V/d$, with d as the distance between the electrodes, we obtain the dependence of the current on the applied bias voltage in the form

$$I(V) \approx A' \exp\left(\frac{q}{kT}\sqrt{\frac{q}{4\pi d\varepsilon_0\varepsilon_S}}\,V^{1/2}\right) = A' \exp(b\,V^{1/2}) \quad (2)$$

We note that the $I(V) \propto \exp(b\,V^{1/2})$ dependence in eq 2 also describes the Poole-Frenkel emission of electrons from positively charged trap states into the conduction band of insulators.[32,33] However, in the case of nanorods connected by Au nanoparticles with few nanometers in diameter this bulk approach might not be appropriate. We therefore evaluate the Schottky barrier lowering related to a conducting sphere where the Coulomb force due to the image charge is given by[34]

$$F(y) = -\frac{1}{4\pi\varepsilon_0\varepsilon_s}\frac{q^2 a}{y^3}\left(1 - \frac{a^2}{y^2}\right) \quad (3)$$

Here y is the distance between q and its image charge $q' = qa/y$, and a is the radius of the conducting sphere. We make the following approximations: $a \ll y$, and that the image q' is located at the surface of the conducting sphere, thus $y = x$, where x is the distance of the charge q from the metal−semiconductor interface. We can then write the image force as

$$F(x) = -\frac{1}{4\pi\varepsilon_0\varepsilon_s}\frac{q^2 a}{x^3} \quad (4)$$

With this image force we obtain the barrier lowering as

$$\Delta\Phi = \frac{3}{2}E^{2/3}\left(\frac{q\,a}{4\pi\varepsilon_0\varepsilon_s}\right)^{1/3} \quad (5)$$

and the distance of the barrier maximum from the Au-nanorod interface is

$$x_m = \left(\frac{q\,a}{4\pi\varepsilon_0\varepsilon_s E}\right)^{1/3} \quad (6)$$

By assuming again a constant electric field, the current−voltage dependence can be expressed as

$$I(V) = B \exp\left[\frac{-q}{kT}\frac{3}{2d^2}\left(\frac{q\,a}{4\pi\varepsilon_0\varepsilon_s}\right)^{1/3} V^{2/3}\right] = B \exp(c\,V^{2/3}) \quad (7)$$

Details of the derivation of the current dependence are shown in the Supporting Information, and a geometrical scheme illustrating the approximation is shown in Figure 4f. Typical current-voltage characteristics recorded at room temperature from network devices before and after annealing are displayed in Figure 4a,c, respectively, together with the fits to the data using eqs 2 and 7. While both fitting models work well at high bias voltage, we find significant differences in the low bias regime from 0 to 4 V. Here the data recorded before annealing can be best described by the bulk Schottky−Richardson model, and from eq 2 we obtain $\varepsilon_S = 1.14$ for the effective permittivity, while fitting with eq 7 yields $\varepsilon_S = 1.3$. On the other hand, after annealing (Figure 4c) the $I-V$ curve can be best fitted over the full voltage range with eq 7 that describes the barrier lowering related to metallic spheres, and from this fit we obtain $\varepsilon_S = 2$. The effective permittivity of CdSe nanorods was predicted by Demchenko *et al.*[18] to be in the range from 10, at the center of the rod, to 1 at the rod surface, and therefore both values are reasonable. We will now discuss why our conducting sphere model (from eq 7) describes the network conduction after annealing well, and fails to describe the current before annealing, where the size of the Au nanoparticles is even smaller. To this end we make some geometrical considerations that show that the assumption of Coulomb attraction due to image charges from a single conducting sphere is not valid. Evaluation of the distance of the Schottky barrier maximum from the metal−semiconductor interface from eq 6 yields $x_m = 5$ nm for a bias voltage of 2 V, assuming a sphere radius of 1 nm. The obtained value of x_m is equal to the nanorod diameter and larger than the average distance between the Au domains on the lateral facets of the nanorods. Therefore the Coulomb forces from multiple Au domains should act on a charge q in the network structures before annealing (as illustrated in Figure 4e), and consequently our model from eq 7 fails to describe the $I-V$ curve. Instead, we find that the square-root-dependence of the bias voltage fits the natural logarithm of the current before annealing well (eq 2), which can be related either to the bulk Schottky, or to the Poole−Frenkel model, as discussed before.

After the annealing process, Au nanoparticles (with radius around 2.5 nm) were solely present in the nanorod junctions, therefore the distance in between the Au nanoparticles was equal to the length of the nanorods that was around 30 nm. The calculation of the distance of the barrier maximum with our approach yields $x_m = 7$ nm in this case, which is considerably smaller than the nanorod length. These values make the assumption of barrier lowering due to a single conducting Au nanoparticle reasonable, and indeed we find that our approximation of the conducting sphere model describes the $I-V$ data after annealing very well over the full bias range (see blue fit curve

in Figure 4c). The good fitting result can be attributed to the appropriate consideration of the image charge, while the rough approximation of $y = x$ might lead to an uncertainty in the calculation of the position of x_m.

At low temperature the thermal activation of carriers should be negligible, and the conductance should be dominated by charge tunneling. The current-voltage curves recorded at $T = 10$ K (Figure 4b,d) show suppression of the current below a certain threshold voltage, and it is reasonable to assume that this effect is due to Coulomb blockade. If we consider 10 junctions in the conductive path, the voltage threshold per junction is around 200−300 mV, which is a reasonable value for the Coulomb charging of nanosize metal particles where the charging energy is determined by the sum of the junction capacitances.[3,35] At bias voltages larger than 3 V the $I-V$ curves can be well described by fitting with exponential functions. Before the annealing process, we could identify two regimes, above and below $V = 8$ V, in which the data could be fitted by two different exponential functions of the form $I(V) = C \exp(V/V_B)$. From our fits we obtained $V_{B1} = 0.73$ V for the low bias range and $V_{B2} = 1.07$ V for the high bias range. In the low bias range the current could be driven by charges filling the trap states, which leads to the voltage barrier value V_{B1}. Once all the traps are filled, the current is determined by the tunnel barriers at the metal−semiconductor interfaces with the barrier voltage V_{B2}. The current−voltage curve after annealing is displayed in Figure 4d, where we observed suppressed conduction up to a bias voltage of 2.5 V and then an exponential increase of the current. We note that the finite current at zero bias voltage is due to an offset in the current amplifier. From our fitting we obtained $V_B = 1.16$ V, which is similar to V_{B2} that we extracted from the high bias regime before annealing, and which confirms the association of these values to the barrier height related to the metal−semiconductor interfaces. Here V_B corresponds to the average of the sum of all the barrier heights of the conductive pathways.

In the following we will analyze the temperature dependence of the network current before and after annealing. Before annealing we observed an anomalous temperature dependence of the current following

$$I(T) \propto \exp(T/T_0) \qquad (8)$$

as demonstrated by the plot of ln(I) *versus* T in Figure 5a, which does not correspond to the expected temperature dependence for thermionic Schottky emission from eq 1. A similar temperature dependence of the current as in eq 8 has been reported by Steinberg *et al.*[10] for CdSe nanorods strongly coupled to tungsten electrodes, and was motivated by temperature-related changes in the CdSe band structure. Hurd[36] reviewed the temperature-dependent conduction in several low-conductivity semiconductors[37,38] and argued that

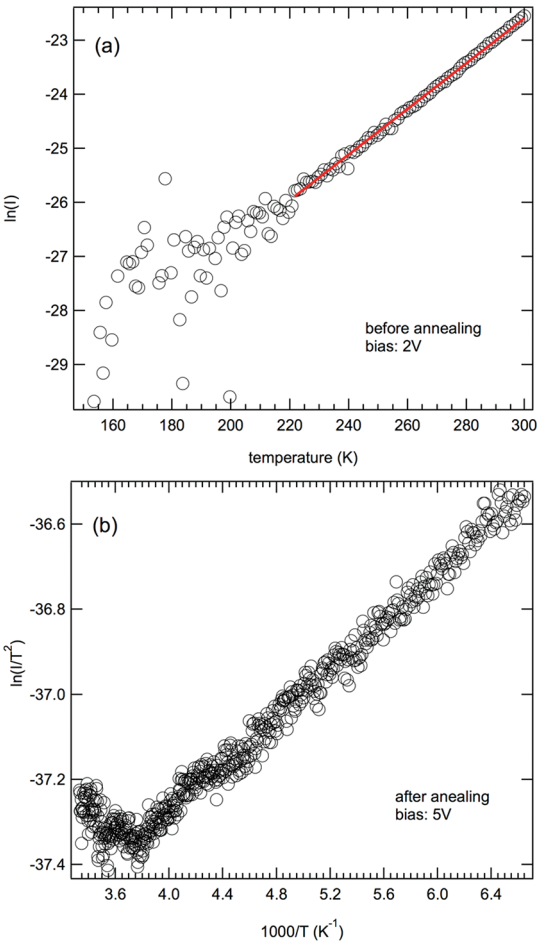

Figure 5. (a) Before the annealing process, the natural logarithm of the current, recorded at a bias voltage of $V = 2$ V, depends linearly on the temperature, and from fitting with eq 8 we obtain $T_0 = 23.6$ K. (b) After the annealing process, the current is plotted as the natural logarithm of I/T^2 *versus* 1000/T, which according to eq 1 should display a linear behavior.

a log(I) ∝ T behavior can be related to quantum tunneling through a vibrating potential barrier with a frequency ω that was assumed as $\omega \approx 10^{12}$ s^{-1}.

After the annealing process, the $I-V$ curves could be well fitted by the thermionic emission model considering the barrier lowering caused by the spherical Au nanoparticles, and therefore we would expect a temperature dependence that follows eq 1. Figure 5b shows a typical temperature dependence of the current (recorded at a bias voltage of 5 V) plotted correspondingly, as ln(I/T^2) *versus* 1/T, where the current follows the expected behavior in a small range at high temperatures (300−260 K). However, the data range is too small to draw any conclusions or to evaluate the barrier height. At low temperatures the data in Figure 5b follows again a linear behavior, but with a positive slope, which needs further clarification. One possible explanation for this atypical temperature dependence could result from different charge transport processes like hopping, tunneling, and thermal emission in different

temperature regimes. We remark that the increase of the conductivity after annealing at low temperature resulted in a crossover of the I(T) curves, which can be seen in the Arrhenius plots of the temperature dependence of the current in Figure S6 of the Supporting Information.

CONCLUSION

We have shown that robust electrical devices based on CdSe nanorods linked into networks *via* Au domains can be fabricated in a simple and reproducible way. The charge transport at room temperature in such networks was dominated by thermionic emission across nanosize Schottky barriers, while at low temperatures it was governed by charge tunneling and Coulomb blockade. The stable conductivity of such all-inorganic networks could pave the way to bottom-up approaches toward complex electronic devices based on colloidal nanoparticles.

METHODS

Nanorod Synthesis and Network Fabrication. The CdSe nanorods were fabricated by coinjection of organo-metallic precursors (Cd and Se) and preformed spherical CdSe nanocrystal seeds with a small size distribution into a reaction flask containing a hot solution (340 °C) of surfactants (trioctylphosphine oxide-(TOPO), octadecylphosphonic acid(ODPA) and hexylphosphonic acid(HPA)). After few minutes, CdSe nanorods with wurtzite crystalline structure were obtained. We then mixed a solution of CdSe nanorods dissolved in toluene (1 mL) with a solution of $AuCl_3$ (50 μL) under the addition of didecyl dimethyl ammonium bromide (DDAB) in toluene in order to obtain the nanodumbells, that is, the CdSe nanorods with Au domains at their tips. Nanorod network structures were formed by injecting small amounts of molecular iodine (I_2) (10 μL) to the CdSe−Au nanodumbbells in solution.

Thermal Annealing of Electrical Devices. The devices were annealed *ex-situ* (inside a glovebox) under N_2 atmosphere at 200 °C for 15 min.

Transmission Electron Microscopy (TEM) Analysis. The samples were prepared by dropping dilute solutions of NCs onto carbon-coated copper grids. Conventional TEM images were recorded on a JEOL JEM 1011 microscope operating at 100 kV. High resolution TEM (HRTEM) and high angular angle dark field (HAADF) scanning TEM (STEM) measurements were performed with a JEOL JEM-2200FS microscope, equipped with a field emission gun working at an accelerating voltage of 200 kV, a CEOS spherical aberration corrector of objective lens allowing to reach a spatial resolution of 0.9 Å, and an in column Omega filter. The annealing experiments were carried out *in situ*, during the observations at a pressure of 10^{-5} Pascal, using a JEOL single tilt heater holder.

Electrode fabrication. We fabricated interdigitated electrodes with 180 nm separation by electron-beam lithography (EBL) on Si/SiO_2 substrates (oxide thickness 200 nm), followed by metal evaporation of 5 nm Ti and 45 nm Au and subsequent lift-off.

Nanocrystal Deposition by Dielectrophoresis. The electrode devices were immersed into a toluene solution that contained the nanoparticles (either CdSe nanorods, nanodumbbells, or networks) at a concentration of 10^{-8} M, and an AC voltage of 5 V_{rms} at 5 kHz was applied for 3 min to the interdigitated electrodes. After the trapping process the devices were transferred into clean toluene solution and then dried by nitrogen flow. All samples were kept in a high vacuum chamber for few days for degassing.

Electrical Measurements. The conductivity of the devices was measured with a Keithley 2612A sourcemeter and a DL Instruments 1211 current preamplifier both on an ambient probe station from Süss Microtech, and under vacuum in a cryogenic Janis Research micromanipulated probe system.

Conflict of Interest: The authors declare no competing financial interest.

Acknowledgment. The authors acknowledge partial financial support from the European Union *via* the FP7 starting ERC Grant NANO-ARCH (Contract No. 240111).

Supporting Information Available: (1) Linear plots of the current−voltage curves before and after annealing; (2) discussion of conducting sphere model for the image charges applied for fitting the *I*−*V* curves recorded at room temperature before and after annealing; (3) HRTEM image of a nanorod junction after annealing that showed an epitaxial relationship; (4) Arrhenius plots of the temperature-dependent current before and after annealing; (5) scanning electron microscopy images of an unbiased interdigitated electrode structure recorded after the network deposition onto a neighboring electrode structure. This material is available free of charge *via* the Internet at http://pubs.acs.org.

REFERENCES AND NOTES

1. Klein, D. L.; McEuen, P. L.; Katari, J. E. B.; Roth, R.; Alivisatos, A. P. An Approach to Electrical Studies of Single Nanocrystals. *Appl. Phys. Lett.* **1996**, *68*, 2574–2576.
2. Klein, D. L.; Roth, R.; Lim, A. K. L.; Alivisatos, A. P.; McEuen, P. L.; Single-Electron, A Transistor Made from a Cadmium Selenide Nanocrystal. *Nature* **1997**, *389*, 699–701.
3. Bezryadin, A.; Dekker, C.; Schmid, G. Electrostatic Trapping of Single Conducting Nanoparticles between Nanoelectrodes. *Appl. Phys. Lett.* **1997**, *71*, 1273–1275.
4. Krahne, R.; Morello, G.; Figuerola, A.; George, C.; Deka, S.; Manna, L. Physical Properties of Elongated Inorganic Nanoparticles. *Phys. Rep.* **2011**, *501*, 75–221.
5. Manna, L.; Scher, E. C.; Alivisatos, A. P. Shape Control of Colloidal Semiconductor Nanocrystals. *J. Cluster Sci.* **2002**, *13*, 521–532.
6. Carbone, L.; Nobile, C.; De Giorgi, M.; Sala, F. D.; Morello, G.; Pompa, P.; Hytch, M.; Snoeck, E.; Fiore, A.; Franchini, I. R.; *et al.* Synthesis and Micrometer-Scale Assembly of Colloidal Cdse/Cds Nanorods Prepared by a Seeded Growth Approach. *Nano Lett.* **2007**, *7*, 2942–2950.
7. Cui, Y.; Banin, U.; Bjork, M. T.; Alivisatos, A. P. Electrical Transport through a Single Nanoscale Semiconductor Branch Point. *Nano Lett.* **2005**, *5*, 1519–1523.
8. Gudiksen, M. S.; Maher, K. N.; Ouyang, L.; Park, H. Electroluminescence from a Single-Nanocrystal Transistor. *Nano Lett.* **2005**, *5*, 2257–2261.
9. Trudeau, P. E.; Sheldon, M.; Altoe, V.; Alivisatos, A. P. Electrical Contacts to Individual Colloidal Semiconductor Nanorods. *Nano Lett.* **2008**, *8*, 1936–1939.
10. Steinberg, H.; Lilach, Y.; Salant, A.; Wolf, O.; Faust, A.; Millo, O.; Banin, U. Anomalous-Temperature Dependent Transport through Single Colloidal Nanorods Strongly Coupled to Metallic Leads. *Nano Lett.* **2009**, *9*, 3671–3675.
11. Steinberg, H.; Wolf, O.; Faust, A.; Salant, A.; Lilach, Y.; Millo, O.; Banin, U. Electrical Current Switching in Single CdSe Nanorods. *Nano Lett.* **2010**, *10*, 2416–2420.
12. Mokari, T.; Rothenberg, E.; Popov, I.; Costi, R.; Banin, U. Selective Growth of Metal Tips onto Semiconductor Quantum Rods and Tetrapods. *Science* **2004**, *304*, 1787–1790.
13. Mokari, T.; Sztrum, C. G.; Salant, A.; Rabani, E.; Banin, U. Formation of Asymmetric One-Sided Metal-Tipped Semiconductor Nanocrystal Dots and Rods. *Nat. Mater.* **2005**, *4*, 855–863.
14. Steiner, D.; Mokari, T.; Banin, U.; Millo, O. Electronic Structure of Metal−Semiconductor Nanojunctions in Gold CdSe Nanodumbbells. *Phys. Rev. Lett.* **2005**, *95*, 056805.

15. Sheldon, M. T.; Trudeau, P.-E.; Mokari, T.; Wang, L.-W.; Alivisatos, A. P. Enhanced Semiconductor Nanocrystal Conductance *via* Solution Grown Contacts. *Nano Lett.* **2009**, *9*, 3676–3682.
16. Landman, U.; Barnett, R. N.; Scherbakov, A. G.; Avouris, P. Metal–Semiconductor Nanocontacts: Silicon Nanowires. *Phys. Rev. Lett.* **2000**, *85*, 1958–1961.
17. Leonard, F.; Talin, A. A. Size-Dependent Effects on Electrical Contacts to Nanotubes and Nanowires. *Phys. Rev. Lett.* **2006**, *97*, 026804.
18. Demchenko, D. O.; Wang, L. W. Localized Electron States near a Metal/Semiconductor Nanocontact. *Nano Lett.* **2007**, *7*, 3219–3222.
19. Romero, H. E.; Calusine, G.; Drndic, M. Current Oscillations, Switching, and Hysteresis in Cdse Nanorod Superlattices. *Phys. Rev. B* **2005**, *72*, 235401.
20. Steiner, D.; Aharoni, A.; Banin, U.; Millo, O. Level Structure of InAs Quantum Dots in Two-Dimensional Assemblies. *Nano Lett.* **2006**, *6*, 2201–2205.
21. Steiner, D.; Azulay, D.; Aharoni, A.; Salant, A.; Banin, U.; Millo, O., Electronic Structure and Self-Assembly of Cross-Linked Semiconductor Nanocrystal Arrays. *Nanotechnology* **2008**, *19*, Article No. 065201.
22. Persano, A.; Leo, G.; Manna, L.; Cola, A., Charge Carrier Transport in Thin Films of Colloidal Cdse Quantum Rods. *J. Appl. Phys.* **2008**, *104*, Article No. 074306.
23. Steiner, D.; Azulay, D.; Aharoni, A.; Salant, A.; Banin, U.; Millo, O. Photoconductivity in Aligned CdSe Nanorod Arrays. *Phys. Rev. B* **2009**, *80*, 195308.
24. Persano, A.; De Giorgi, M.; Fiore, A.; Cingolani, R.; Manna, L.; Cola, A.; Krahne, R. Photoconduction Properties in Aligned Assemblies of Colloidal CdSe/CdS Nanorods. *ACS Nano* **2010**, *4*, 1646–1652.
25. Rivest, J. B.; Swisher, S. L.; Fong, L.-K.; Zheng, H.; Alivisatos, A. P. Assembled Monolayer Nanorod Heterojunctions. *ACS Nano* **2011**, *5*, 3811–3816.
26. Kelly, D.; Singh, A.; Barrett, C. A.; O'Sullivan, C.; Coughlan, C.; Laffir, F. R.; O'Dwyer, C.; Ryan, K. M. A Facile Spin-Cast Route for Cation Exchange of Multilayer Perpendicularly-Aligned Nanorod Assemblies. *Nanoscale* **2011**, *3*, 4580–4583.
27. Figuerola, A.; Franchini, I. R.; Fiore, A.; Mastria, R.; Falqui, A.; Bertoni, G.; Bals, S.; Van Tendeloo, G.; Kudera, S.; Cingolani, A.; *et al.* End-to-End Assembly of Shape-Controlled Nanocrystals *via* a Nanowelding Approach Mediated by Gold Domains. *Adv. Mater.* **2009**, *21*, 550–554.
28. Figuerola, A.; Huis, M. v.; Zanella, M.; Genovese, A.; Marras, S.; Falqui, A.; Zandbergen, H. W.; Cingolani, R.; Manna, L. Epitaxial CdSe-Au Nanocrystal Heterostructures by Thermal Annealing. *Nano Lett.* **2010**, *10*, 3028–3036.
29. Franchini, I. R.; Cola, A.; Rizzo, A.; Mastria, R.; Persano, A.; Krahne, R.; Genovese, A.; Falqui, A.; Baranov, D.; Gigli, G.; Manna, L. Phototransport in Networks of Tetrapod-Shaped Colloidal Semiconductor Nanocrystals. *Nanoscale* **2010**, *2*, 2171–2179.
30. Zhang, Y.; Miszta, K.; Kudera, S.; Manna, L.; Di Fabrizio, E.; Krahne, R. Spatially Resolved Photoconductivity of Thin Films Formed by Colloidal Octapod-Shaped CdSe/CdS Nanocrystals. *Nanoscale* **2011**, *3*, 2964–2970.
31. Sze, S. M.; Kwok, K. N. *Physics of Semiconductor Devices*; 3rd ed.; Wiley: Hoboken, NJ, 2007.
32. Simmons, J. G. Poole–Frenkel Effect and Schottky Effect in Metal–Insulator–Metal Systems. *Phys. Rev.* **1967**, *155*, 657.
33. Ganichev, S. D.; Ziemann, E.; Prettl, W.; Yassievich, I. N.; Istratov, A. A.; Weber, E. R. Distinction between the Poole–Frenkel and Tunneling Models of Electric-Field-Stimulated Carrier Emission from Deep Levels in Semiconductors. *Phys. Rev. B* **2000**, *61*, 10361.
34. Jackson, J. D. *Classical Electrodynamics*; 3rd ed.; Wiley: New York, 1999.
35. Grabert, H.; Devoret, M. H. *Single Charge Tunneling—Coulomb Blockade Phenomena in Nanostructures*; Kluwer Academic/Plenum Publisher: New York, 1992.
36. Hurd, C. M. Quantum Tunneling and the Temperature-Dependent DC Conduction in Low-Conductivity Semiconductors. *J. Phys. C* **1985**, *18*, 6487–6499.
37. Pistoulet, B.; Roche, F. M.; Abdalla, S. AC Band Conductivity in Compensated Semiconductors with Potential Fluctuations. *Phys. Rev. B* **1984**, *30*, 5987–5999.
38. Garciacuenca, M. V.; Morenza, J. L.; Codina, J. M. On the Hall-Effect in Polycrystalline Semiconductors. *J. Appl. Phys.* **1985**, *58*, 1080–1082.